The Astronomical Journal, 144:147 (11pp), 2012 November doi:10.1088/0004-6256/144/5/147

KRONBERGER 49: A NEW LOW-MASS GLOBULAR CLUSTER OR AN UNPRECEDENTED BULGE WINDOW?*

S. Ortolani[1,7], C. Bonatto[2], E. Bica[2], B. Barbuy[3], and R. K. Saito[4,5,6]
[1] Dipartimento di Astronomia, Università di Padova, Vicolo dell'Osservatorio 5, I-35122 Padova, Italy; ortolani@pd.astro.it
[2] Departamento de Astronomia, Universidade Federal do Rio Grande do Sul, CP 15051, Porto Alegre 91501-970, Brazil; charles.bonatto@ufrgs.br, bica@if.ufrgs.br
[3] Departamento de Astronomia, Universidade de São Paulo, Rua do Matão 1226, São Paulo 05508-900, Brazil; barbuy@astro.iag.usp.br
[4] Departamento de Astronomía y Astrofísica, Pontificia Universidad Católica de Chile, Vicuña Mackenna 4860, Casilla 306, Santiago 22, Chile; rsaito@astro.puc.cl
[5] Departamento de Física y Astronomía, Facultad de Ciencias, Universidad de Valparaíso, Ave. Gran Bretaña 1111, Playa Ancha, Casilla 5030, Valparaíso, Chile
[6] The Milky Way Millennium Nucleus, Av. Vicuña Mackenna 4860, 782-0436 Macul, Santiago, Chile
Received 2012 March 19; accepted 2012 September 7; published 2012 October 11

ABSTRACT

We employ optical and near-infrared photometry to study the stars in the direction of the star cluster candidate Kronberger 49. The optical color–magnitude diagrams (*V*, *I*, and Gunn *z* photometry obtained with the Galileo Telescope) are tight and present evidence of a main-sequence turnoff. We may be dealing with a low-mass, metal-rich globular cluster located in the bulge at a distance from the Sun of $d_\odot = 8 \pm 1$ kpc. Alternatively, it may be a dust hole through which we are sampling the bulge stellar population affected by a very low amount of differential reddening.

Key words: globular clusters: individual (Kronberger 49) – Hertzsprung–Russell and C–M diagrams

Online-only material: color figures

1. INTRODUCTION

New globular clusters have been recently revealed from large sky surveys, which add to the list of 157 objects reported in Harris' (1996, 2010 edition) globular cluster catalog.[8] The newly identified globular clusters in the direction of the bulge, VVV CL001 (Minniti et al. 2011) and VVV CL002 (Moni Bidin et al. 2011), were revealed by the VISTA Variables in the Via Lactea (VVV) survey (Minniti et al. 2010); SEGUE 3 is a very low mass star cluster in the halo, revealed by the SDSS/SEGUE survey (Fadely et al. 2011). Not surprisingly, they are in general faint, poorly populated, and in the case of the bulge, heavily field-contaminated. Given that the population of Galactic globular clusters is intrinsically small, new additions are important for the understanding of their formation and evolution processes.

The inspection of color–magnitude diagrams (CMDs) of star clusters unclassified in the past, such as AL 3 and Pfleiderer 2 (Ortolani et al. 2006, 2009, and references therein), led to the identification of these objects as globular clusters.

Bulge directions are heavily affected by high and variable extinction (e.g., Dutra et al. 2003) that hamper observation of the intrinsic bulge stellar population. However, several large ($\sim 1^\circ$) windows have been found, e.g., Baade's Window (Baade & Gaposchkin 1963) and two others discovered by Dutra et al. (2002). Even when looking through a window, the CMDs are usually scattered by differential reddening. For instance, the optical study of Terndrup (1988) shows a relatively wide color range in CMDs of the stellar population within Baade's Window and of other Galactic latitude directions crossing the bulge. Baade's Window contains two globular clusters, the intermediate-metallicity NGC 6522 ($d_\odot = 7.7$ kpc and $A_V = 1.5$) near the window center and the metal-rich NGC 6528 ($d_\odot = 7.9$ kpc and $A_V = 1.6$) to the edge. Both are projected relatively high in the bulge, at $b \approx -4^\circ$.

Kronberger et al. (2006) presented a list of star cluster candidates, based on DSS/XDSS and Two Micron All Sky Survey (2MASS) images. Inspection of such images shows a compact object, suggesting the core of a globular cluster, and for this reason we decided to observe Kronberger 49 (also designated as J1810.3−2320) at the Telescopio Nazionale Galileo (TNG). Kronberger 49 is located at J2000 $\alpha = 18^{\rm h}10^{\rm m}23\overset{\rm s}{.}9$, $\delta = -23^\circ 20' 25''$, with Galactic coordinates $\ell = 7\overset{\circ}{.}63$, $b = -2\overset{\circ}{.}01$. Thus, the present direction occurs at a lower latitude than the globular clusters in Baade's Window.

The present paper is based mainly on *V*, *I*, and Gunn *z* photometry obtained with TNG (Section 2). However, we also employ additional photometry from 2MASS (Skrutskie et al. 2006), the Deep Near Infrared Survey of the Southern Sky (DENIS; The DENIS Consortium 2005), the *Wide-field Infrared Survey Explorer* (*WISE*; Wright et al. 2010), and VVV (Minniti et al. 2010) in order to identify the CMD sequences and constrain the nature of this object. In Section 2, the TNG observations and reductions are described. In Section 3, the TNG CMDs are analyzed. In Section 4, we discuss additional photometry available for the object Kronberger 49. Finally, Section 5 summarizes the results.

2. OBSERVATIONS

The direction of Kronberger 49 was observed on 2011 June 23–24, with the 3.58 m TNG telescope at La Palma, equipped with the Dolores spectrograph focal reducer. An EEV 4260 CCD detector with 2048×2048 pixels, of pixel size 13 μm was employed. A pixel corresponds to $0\overset{''}{.}252$ on the sky, and the

* Based on observations made with the Italian Telescopio Nazionale Galileo (TNG) operated on the island of La Palma, by the Fundación Galileo Galilei of INAF (Istituto Nazionale di Astrofisica) at the Spanish Observatorio del Roque de los Muchachos of the Instituto de Astrofisica de Canarias.
7 Visiting Astronomer, Telescopio Nazionale Galileo (TNG), La Palma, Canary Islands, Spain.
8 http://www.physics.mcmaster.ca/Globular.html

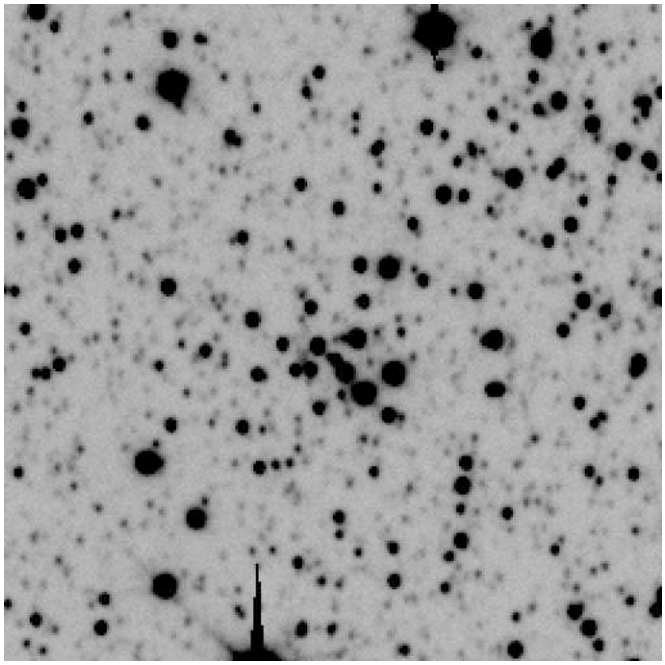

Figure 1. Kronberger 49: 60 s exposure in *I*. Extraction of $\sim 2' \times 2'$. A stellar cluster or the central region of a bulge dust window? North is up and east is left.

Table 1
Log of Observations

Filter	Date	Exp (s)	Seeing (″)	Airmass
I	2011 Jun 23–24	30	1.0	1.6
I	”	300	0.9	1.6
I	”	60	0.7	1.6
V	”	120	0.9	1.7
V	”	900	1.0	1.6
z	”	60	1.0	1.6
z	”	30	1.0	1.6

full field of the camera is $8\farcm6 \times 8\farcm6$. The log of observations is given in Table 1. Figure 1 shows a 60 s *I* image of Kronberger 49, for an extraction of $2' \times 2'$, basically corresponding to the central part of the full image.

2.1. Calibrations and Reductions

The calibration was performed using two different Landolt (1992) standard fields observed in V, I (PG1528, PG 2213) with various exposure times and in different positions on the frame to check for systematics across the field. We also checked the accuracy of the shutter time. The airmass corrections of 0.15 mag airmass^{-1} in *V*, and 0.07 in *I*, have been applied using the standard values given for La Palma on clear nights (without dust in the atmosphere), available at the DOLORES Web site.[9]

The derived calibration equations are

$$V = 29.1 - 0.03(V - I) + v$$

$$I = 28.75 - 0.09(V - I) + i,$$

[9] http://www.tng.iac.es/info/la_palma_sky.html

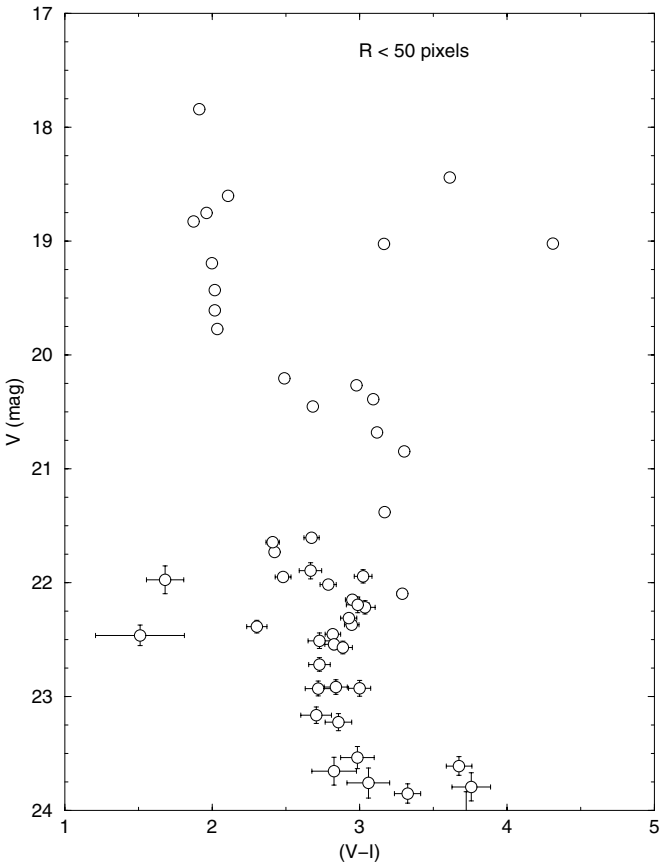

Figure 2. TNG photometry extracted from the central 50 pixels (13″) of Kronberger 49.

where the zero points are calculated for 15 s in *I* and 20 s in *V* exposures at 1.1 airmasses, with an aperture of 40 × 40 pixels. *v* and *i* are instrumental magnitudes (counts in ADUs, gain 1 e^-/ADU), while *V* and *I* are the calibrated ones. No shutter time effects have been detected at the 0.01 mag level in the exposure range of our images (from 1 to 20 s). The repeated measurements of the standard stars across the field allowed us to detect the photometric errors induced by the correction with the flat fields affected by sky concentration (Andersen et al. 1995), and to separate this effect from vignetting. The Gunn *z* photometry was not calibrated for the zero point.

CCD frame reductions were performed using a standard flat-field procedure, and the sky concentration effect was corrected in a second step on the extracted photometry. We subtracted 0.03 mag at the center, with a linear interpolation reaching zero at a radius of $R = 600$ pixels. In this position the sky concentration becomes negligible, as derived from the multiple standard star exposures.

The images have been processed with DAOPHOT II and Allstars (Stetson 1987; Stetson 1994). The software is available in MIDAS for the instrumental photometry of individual stars, and it was converted into the standard Johnson–Cousins system, defined from the Landolt stars, using the above calibration equations. The conversion from the instrumental (point-spread function convolved) magnitudes to the calibrated ones revealed an image quality variation across the field. This produces a variable aperture correction, changing with time and filter. The resulting accuracy of the calibration, taking into account the uncertainties in the calibration equations ($\sim$0.01 mag), the flat-fielding

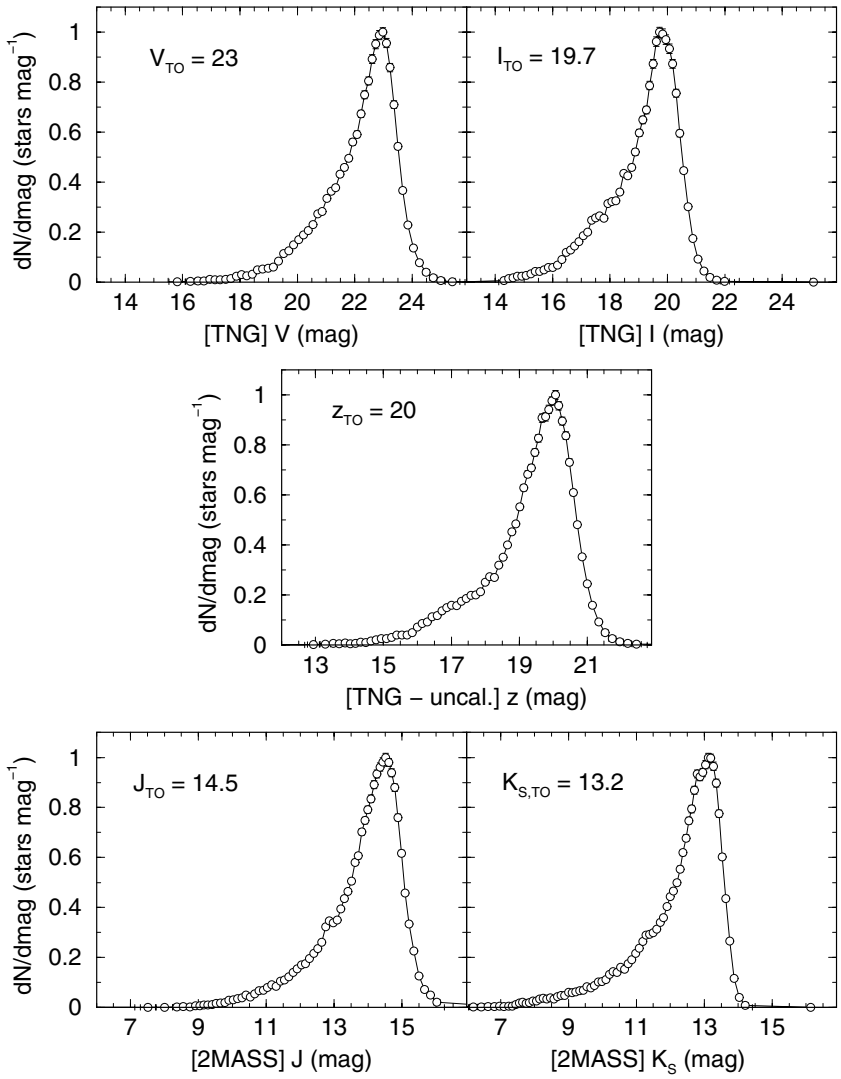

Figure 3. Star counts of the TNG and 2MASS bands are used to investigate the photometric completeness toward Kronberger 49. Note that TNG's z band is not corrected for the zero point. We take the turnover (TO) magnitude as the completeness limit.

procedure (an additional 0.01–0.02 mag) and the aperture corrections (0.02 mag), is estimated to be within ±0.04 in a single filter. The relative photometric errors have been derived from a frame-to-frame photometry comparison with the same filter, using short exposures (120 s in V) compared to the long ones. The errors in V are 0.03 mag for $14 < V < 16.5$, increasing to about 0.2 mag at $V = 23$. In order to obtain the errors for the deeper exposures, these must be scaled according to the corresponding exposure times. Further details can be found in Ortolani et al. (2009).

A first glimpse on the nature of Kronberger 49 is provided by the CMD extracted from a very central region. Figure 2 shows the $V \times (V - I)$ CMD corresponding to the region $R < 52$ pixels (13.″1). The presence of a tight turnoff (at $V \approx 22.6$) is clear, suggesting a star cluster, which is different from the wide color range expected for the bulge (e.g., Terndrup 1988). In addition, the field-star contamination (mostly bulge) is prominent (see the middle panels of Figures 4 and 5), to the point that to assess any CMD properties, decontamination is mandatory. Thus, a fundamental issue in the present study is whether the tight turnoff in Figure 2 indeed corresponds to a globular cluster or an unprecedented bulge stellar population sampling.

2.2. Photometric Completeness

Before proceeding to a deeper analysis of CMDs obtained in the direction of Kronberger 49, we now investigate the photometric completeness of TNG (and 2MASS) by means of star counts in the available bands, i.e., the luminosity functions. They are shown in Figure 3 for V, I, and (the uncalibrated) z bands. Assuming that the turnover magnitude represents the completeness limit for each band, the TNG photometry of Kronberger 49 is essentially complete for stars with $V \lesssim 23$, $I \lesssim 19.7$, and $z \lesssim 20$.

According to specifications,[10] 2MASS is expected to be complete for $J \lesssim 14$ and $K_S \lesssim 13$ at the Galactic latitude of Kronberger 49. Indeed, the J and K_S luminosity functions (Figure 3) present turnovers that agree with the expectations, $J_{TO} = 14.5$ and $K_{S,TO} = 13.2$. As a caveat, we note that

[10] www.astro.caltech.edu/~jmc/2mass/v3/gp/

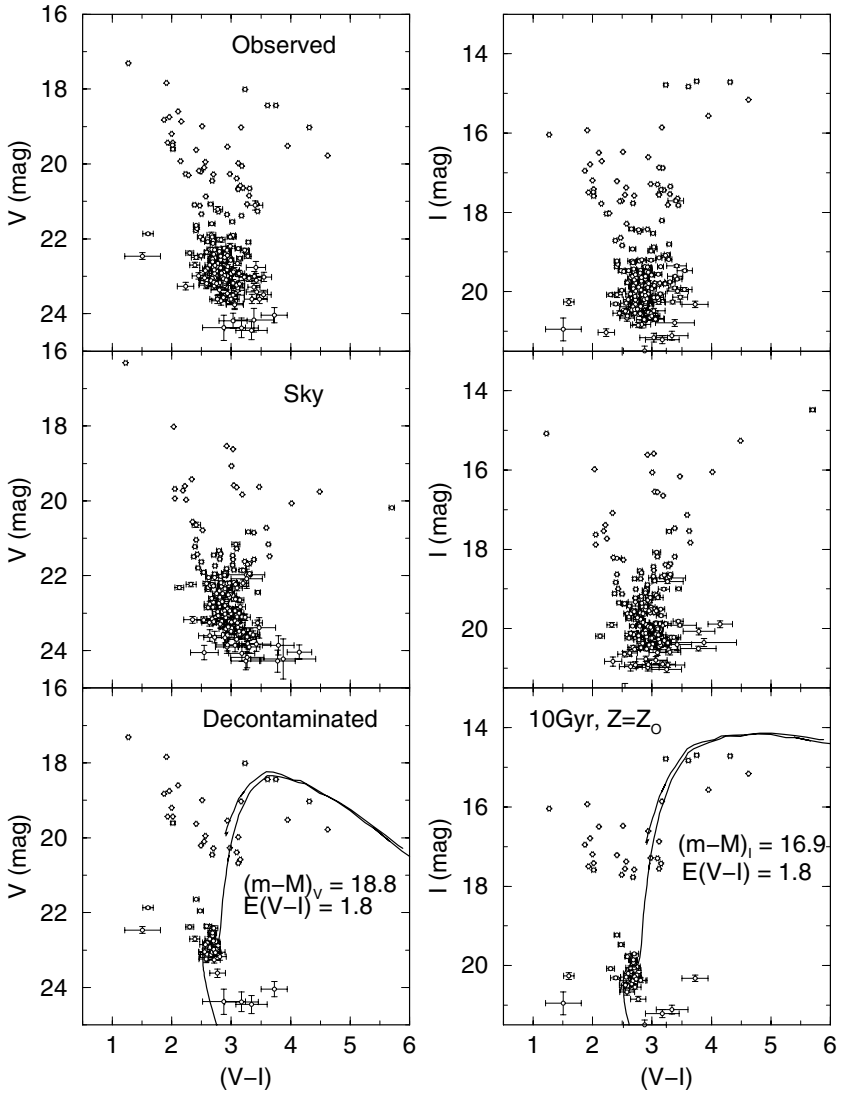

Figure 4. TNG V, I photometry extracted within 100 pixels (≈25″) around the center of the object Kronberger 49. Panels show the observed (top), equal-area comparison field (middle), and statistically subtracted (bottom) CMDs. Padova isochrones for solar metallicity and 10 Gyr are overplotted.

these values should displace a little toward brighter limits when considering dense clusters, for which crowding is more important than for field stars.

2.3. Field-star Decontamination

Field stars can be major contaminants of CMDs, especially for targets projected toward the bulge and/or disk. The decontamination algorithm employed here is based on a statistical routine designed for the wide-field photometry of 2MASS data, as developed in Bonatto & Bica (2007, 2010), and the adaptation of this code to TNG photometry is described in Ortolani et al. (2009). As a technical point, we note that the default color bin size is 0.5 mag (more than two times larger than that used in Ortolani et al. 2009) to account for the relatively low stellar statistics at bright CMD cells of Kronberger 49. In addition, the decontamination also takes color (and magnitude) bins half and twice the default size into account. In the end, the decontaminated CMD corresponds to the average of (equal number of) runs with color bin sizes set at 0.25, 0.5, and 1 mag.

Given the relatively restricted available TNG field, we have used the ring located within 1.′6–1.′9 as comparison field for decontamination purposes.

3. COLOR–MAGNITUDE DIAGRAMS

Figure 4 shows the $V \times (V - I)$ and $I \times (V - I)$, for a cluster extraction of $R = 100$ pixels (25.″2). The upper panel shows the cluster and bulge populations together. In the middle panel a ring sky of equal area is shown, and in the lower panel the decontaminated CMD is presented. The prominent features are a well-defined turnoff and a red giant branch (RGB) with a turnover suggesting high metallicity (Ortolani et al. 1990; Ortolani et al. 1991). The turnoff is low at $V \approx 22.5$, and the diagram follows a 10 Gyr (or older) and $Z = Z_\odot$ Padova isochrone (Marigo et al. 2008). The fit provides the cluster parameters distance modulus of $(m - M)_V = 18.8$, $(m - M)_I = 16.9$, and $E(V - I) = 1.8$, corresponding to a reddening value $E(B - V) = 1.35$. These values lead to a distance from the Sun of $d_\odot = 8 \pm 1$ kpc, thus compatible with the bulge. This metal-rich interpretation, which is equally

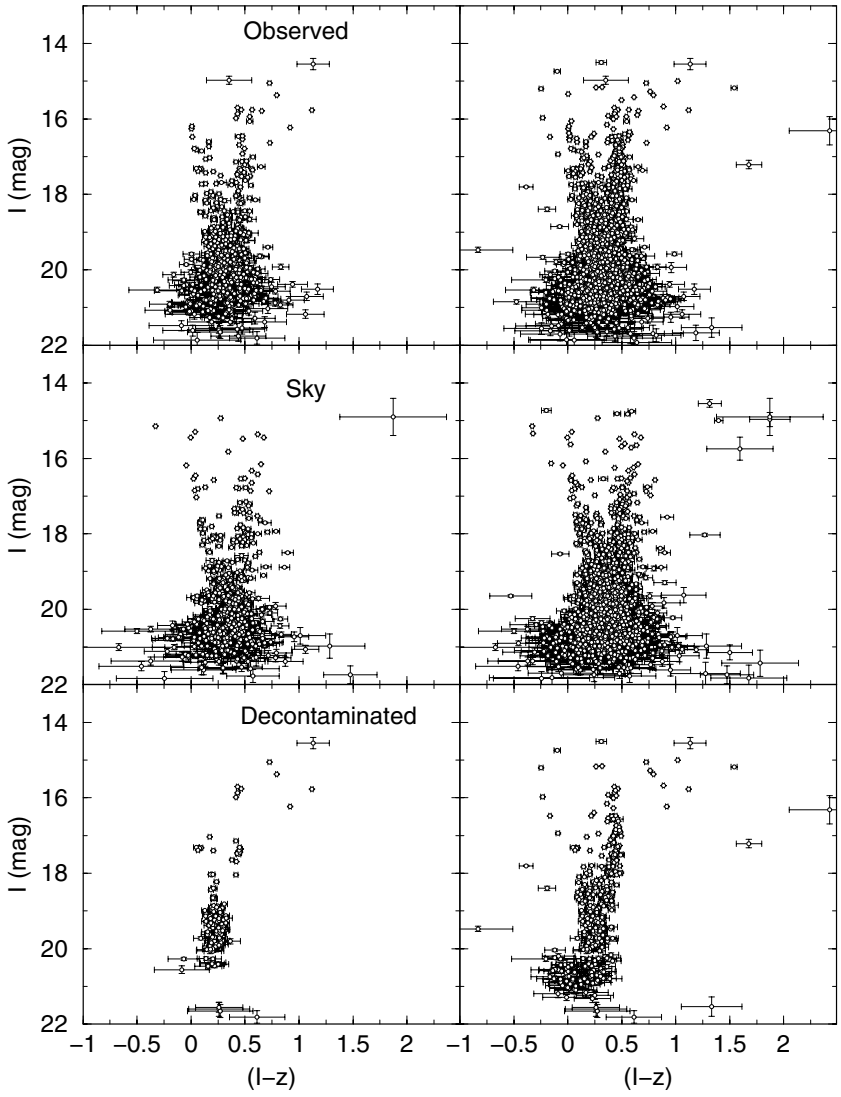

Figure 5. Similar to Figure 4 for the TNG I, z photometry extracted within 150 and 250 pixels (38″ and 63″, respectively).

valid for a globular cluster or a bulge stellar population, is also consistent with forthcoming diagrams.

In Figure 5, the $I \times (I - z)$ diagrams are shown for two apertures of $R = 150$ and 250 pixels (38″ and 63″). Similar to Figure 4, the panels correspond to all stars, field stars, and decontaminated diagrams from top to bottom. In the two upper panels a disk component is clearly seen, as expected since the cluster is located at $b \sim -2.^{\circ}01$. There is no evidence of the blue horizontal branch. An RGB inclination similar to that of NGC 6528 points to a solar-like metallicity (see discussion in Ortolani et al. 1991). These are among the most metal-rich globular clusters in the Galaxy (Harris 1996, 2010 edition). Given the RGB similarity with NGC 6528, we adopt [Fe/H] ≈ -0.1 for Kronberger 49.

Figure 6 shows the 2MASS $J \times (J - K_S)$ diagram, again following the panel distribution of Figures 4 and 5. However, because of the wide field provided by 2MASS, we have used the ring between 10′ and 20′ as comparison field, which also yields an adequate statistical stellar basis for the decontamination. Left and right panels correspond to extractions of $R = 70''$ and 140″, respectively. The decontaminated CMDs present a feature compatible with a globular cluster RGB, which is consistently matched by the isochrone solution obtained with TNG photometry (Figure 4). The high statistical significance of the wide-field stellar background indicates that the subtracted giants imply a low-mass globular cluster.

According to the photometric completeness analysis (Section 2.2), the sharp decrease in the number of stars with $V \gtrsim 23$ and $I \gtrsim 20$ in the decontaminated TNG CMDs (Figures 4 and 5) probably arises from the different completeness limits between cluster and field for faint stars. The same argument applies to the decontaminated 2MASS CMDs (Figure 6) for stars fainter than $J \approx 14.5$.

In the case of a cluster, the absolute magnitude can be estimated by two methods based on the 2MASS photometry: the first one considers the total flux produced by the cluster's giants subtracted from the equivalent one measured in the comparison field (after scaling for the different projected areas); in the second method we compare the number of RGB stars in the field-star decontaminated CMDs with the equivalent one measured in a nearby, relatively uncrowded globular cluster. Taking M 4 (NGC 6121) as a reference cluster with $M_V = -7.19$, we

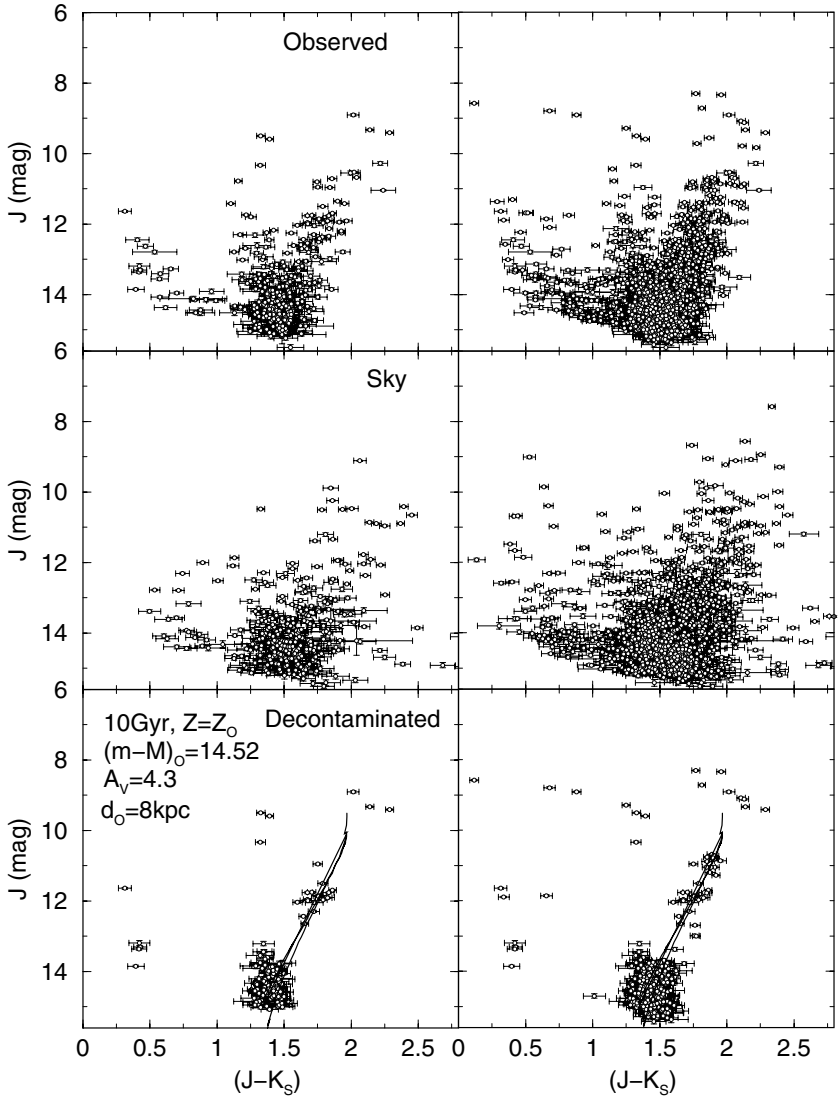

Figure 6. Similar to Figure 4 for the 2MASS photometry extracted within the radii $R = 120$ and 240 pixels (70″ and 140″). The 10 Gyr, solar-metallicity Padova isochrone has been set to the decontaminated CMDs according to the fundamental parameters derived with the TNG photometry (Section 3 and Figure 4).

derive $M_V = -5.4 \pm 0.5$ and -4.8 ± 0.5 from each method, respectively. This would be among the least massive globular clusters in the bulge, comparable, for example, to AL 3, which was identified as a globular cluster in the last decade with $M_V = -4.19$ (Ortolani et al. 2006; Harris 1996, 2010 edition). Interestingly, the latter compilation contains about 20 globular clusters fainter (in absolute terms) than our estimate for Kronberger 49, with the faintest ones located in the halo.

Assuming the distance of the Sun to the Galaxy center as $R_\odot = 8.28$ kpc (Gillessen et al. 2009), the Galactocentric coordinates are $X = -0.35$ kpc (with positive X corresponding to the other side of the Galaxy), $Y = 1.1$ kpc and $Z = -0.28$ kpc. The distance from the Galactic center is $R_{GC} = 1.2$ kpc, thus Kronberger 49 would be an inner bulge cluster.

Finally, Figure 7 shows the radial density profile (stars arcmin^{-2}) built with the TNG VI photometry of Kronberger 49. The very central parts suggest a dense core, but crowding and statistical uncertainties are significant. We might be dealing with a core collapse globular cluster like many others in the central parts of the Galaxy (Trager et al. 1995).

4. ADDITIONAL PHOTOMETRY

Given the intrinsic difficulties associated with the TNG (and 2MASS) analysis of Kronberger 49, we now make use of additional—independent—photometry available around the target region to check and/or constrain our findings. We start with the DENIS I and J data (Figure 8), extracted for the 1′ around Kronberger 49. This region clearly presents an excess of stars at $(I - J) \sim 2.5$ and $I \sim 16$–17 with respect to the field, which is confirmed by the decontamination. When compared to a CMD extracted from the central region of 47 Tuc (NGC 104, set to the same distance as Kronberger 49), we see that both sequences are compatible with the RGB—although with a considerably lower number of stars in Kronberger 49. We note that, to avoid the expected heavy crowding in the central region, the CMD of 47 Tuc was extracted within the ring located at $R = 3'$–$4'$. In addition, this analysis suggests that Kronberger 49 may be a little more metal-rich than 47 Tuc ([Fe/H] $= -0.72$; Harris 1996). Next, we employ the *WISE* $W1$ (3.35 μm) and $W2$ (4.6 μm) bands, which have the

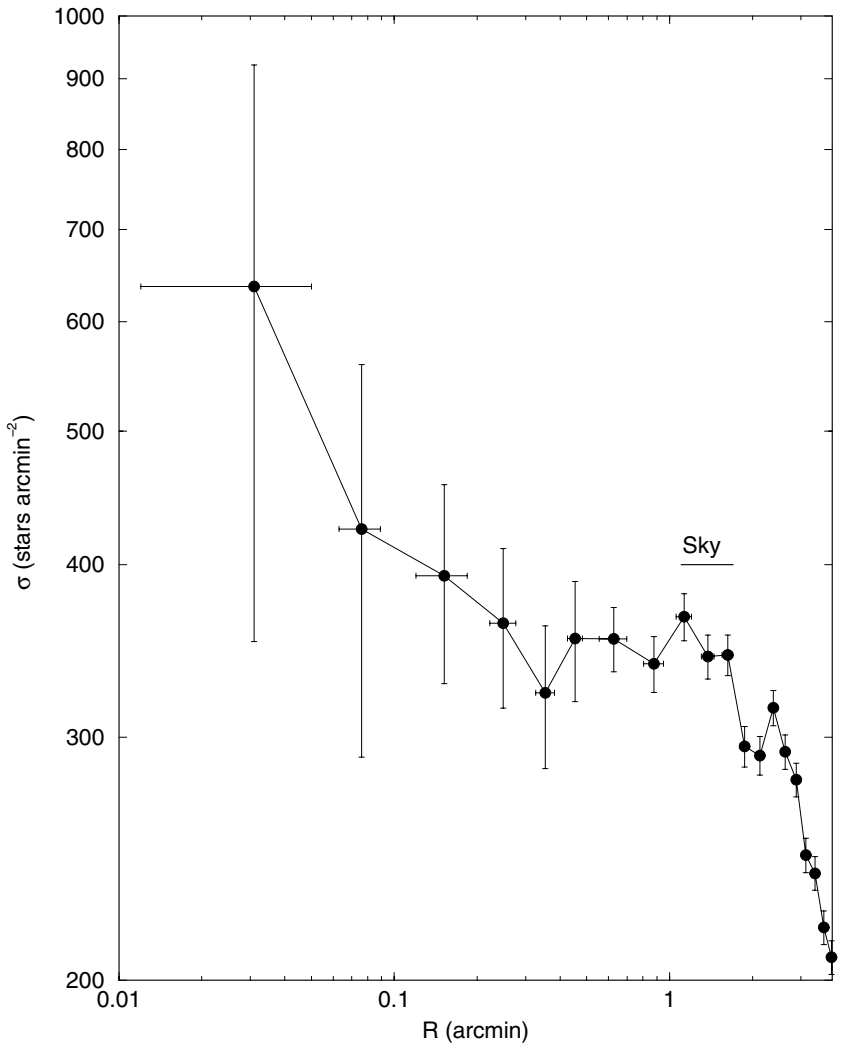

Figure 7. Radial density profile (stars per arcmin^2 vs. radius in arcmin) built with TNG VI photometry for the stars in Kronberger 49. The background sky region for the counts is indicated.

advantage of minimizing reddening effects. The resulting CMDs (Figure 8), although shallower than the DENIS ones, are compatible with Kronberger 49 being a poorly populated globular cluster.

Finally, the rather deep photometry of VVV has already been used to find a few globular clusters in the Galaxy (e.g., Moni Bidin et al. 2011). Since Kronberger 49 lies within the area already surveyed by VVV, we use its J and K_S observations as additional constraint to the nature of this previously known object (Section 1). The resulting VVV CMD for the central $1'$ is shown in Figure 9, where it is compared with the decontaminated 2MASS photometry for the same region. Although VVV reaches about 3 mag deeper in J than 2MASS, and saturates for $J \sim 12$ in this field (stars not included in the CMD), both CMDs are compatible with our identification of a metal-rich population RGB (Section 3).

4.1. A Dust Window?

The Galactic bulge and central disk are characterized by non-uniform dust distributions (e.g., Gonzalez et al. 2012), and the presence of a dust window—through which the bulge population could be seen much deeper than the surroundings—might produce a stellar distribution resembling that of a globular cluster (e.g., Terndrup 1988). To investigate whether the dust window scenario applies to Kronberger 49, we build a color map for the stars observed with TNG. The map (Figure 10) shows the mean $(V-I)$ color in cells of dimension $5'' \times 5''$. The mean color is the color sum of all stars in a given cell divided by the corresponding number of stars. Obviously, a single color is not a direct indication of extinction, but the presence of a dust window should produce systematic color deviations inside it, roughly similar to what occurs in the southeast corner of Figure 10. However, this systematic effect is not present in the central arcmin (corresponding to the estimated dimension of Kronberger 49).

However, the composite *WISE* image (Figure 11) shows the presence of a bubble in the warm dust distribution around Kronberger 49. But, we emphasize that the inner bubble radius ($7' \times 3'.5$) fully encompasses the estimated cluster dimension ($R \sim 1'$; Figure 7) similar to the case of NGC 6522 in Baade's Window. Thus, a globular cluster can occur within a window, although in the present case, it is a factor of 3–4 smaller in radius than Baade's Window.

A different point of view is that we are looking directly the bulge stellar population through a small-scale dust window, and

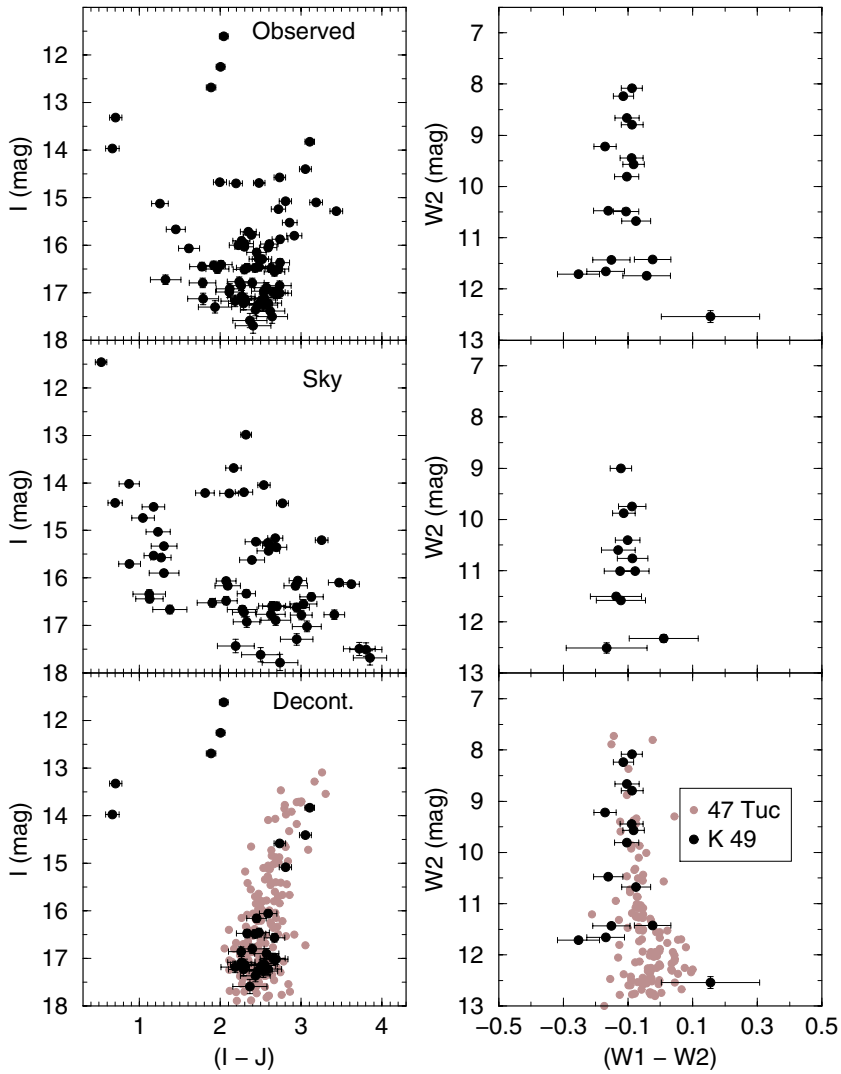

Figure 8. CMDs built with DENIS (left panels) and *WISE* (right) photometry for an extraction of radius 1′ around the object Kronberger 49 (top panels). In both cases the comparison field for decontamination corresponds to the ring located at 20′–30′ (equal-area sky extractions are shown in the middle panels). The decontaminated CMDs (bottom) are compared to 47 Tuc.

(A color version of this figure is available in the online journal.)

the very radial structure of the bubble would be emulating a star cluster CMD. In that case, we would be dealing with an unprecedented sampling of the bulge stellar population at about $b \approx 2^{\circ}$, affected by a very low differential reddening.

5. CONCLUDING REMARKS

Optical photometry from TNG—complemented with near-IR observations from 2MASS, *WISE*, DENIS, and VVV—indicates two possibilities for Kronberger 49. It may be a low-mass, metal-rich globular cluster dwelling in the Galactic bulge or a sample of the bulge stellar population (with an unprecedented low differential reddening) seen through a dust window. The TNG CMDs reach the main-sequence turnoff, showing features compatible with a 10 Gyr—or older—stellar population.

Based on the curved RGB morphology (which basically follows those of NGC 6528 and NGC 6553), we estimate a metallicity of [Fe/H] ≈ -0.1. Such a stellar population is significantly absorbed, with a foreground $A_V \approx 4.2$. It is located in the inner bulge, at a distance $d_{\odot} = 8 \pm 1$ kpc. However, this value is based on the assumed average total-to-selective extinction ratio $R_V = 3.1$. Recently, Zagury (2012) pointed out that R_V may be as high as 4, which would put the object Kronberger 49 at a distance of $d_{\odot} \approx 5.1$ kpc.

In the case of a globular cluster, independent methods lead to an absolute magnitude $M_V = -5.1 \pm 0.3$, which would imply that Kronberger 49 is one of the least-massive globular clusters in the bulge (Harris 1996, 2010 edition). However, it would still be more massive than several halo globular clusters (Siegel et al. 2001; Inman & Carney 1987).

At this point it might be interesting to examine the present census of globular clusters in the bulge direction. Harris (1996, 2010 edition) condenses efforts of the last decades, which we show in Figure 12, where the bulge concentration is clear. We have added to Harris' catalog a few globular clusters recently discovered or identified that complement his list. They are VVV CL001 (Minniti et al. 2011), Mercer 5 (Longmore et al. 2011), Pfleiderer 2 (Ortolani et al. 2009), FSR 1767 (Bonatto

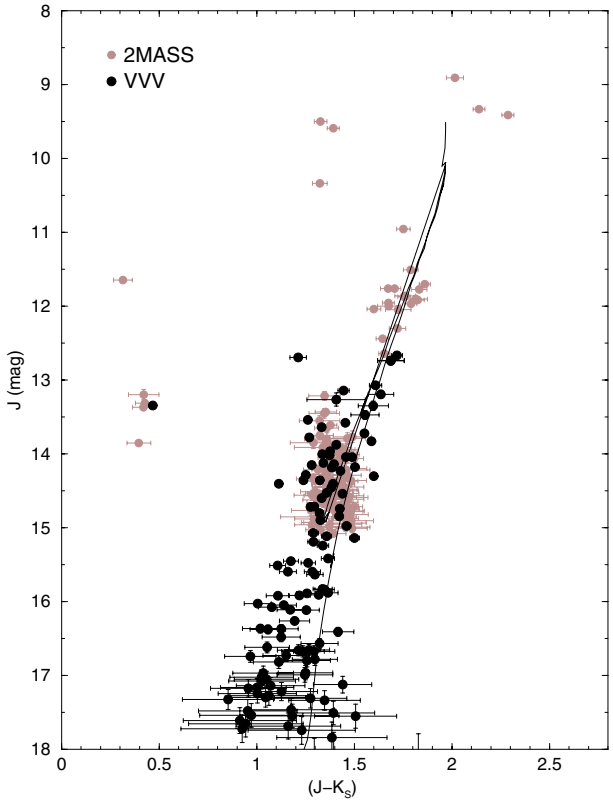

Figure 9. VVV and 2MASS photometry extracted within the central 1′ of Kronberger 49. The VVV colors were transformed from the natural VISTA Vegamag system to the 2MASS system. Isochrone (10 Gyr, solar metallicity) set with the same parameters as in Figure 6.

(A color version of this figure is available in the online journal.)

et al. 2009), and VVV CL002 (Moni Bidin et al. 2011). The object Kronberger 49 is located near the edge of the bulge region studied by Barbuy et al. (1998), which contained at that time 17 clusters. Thus, Kronberger 49 would be a very important addition to the bulge globular cluster population that may eventually be used to better define the structure of the bulge itself. With deep spectroscopy and photometry, Kronberger 49 can also be used to further explore the bulge distribution of abundances and ages.

We thank an anonymous referee for comments and suggestions. We gratefully acknowledge use of data from the ESO VISTA Public Survey VVV, program ID 179.B-2002, taken with the VISTA telescope, and data products from the Cambridge Astronomical Survey Unit. This publication makes use of data products from the *Wide-field Infrared Survey Explorer*, which is a joint project of the University of California, Los Angeles, and the Jet Propulsion Laboratory/California Institute of Technology, funded by the National Aeronautics and Space Administration. We also use data products from the Two Micron All Sky Survey, which is a joint project of the University of Massachusetts and the Infrared Processing and Analysis Center/California Institute of Technology, funded by the National Aeronautics and Space Administration and the National Science Foundation. We acknowledge partial financial support from the Brazilian agencies CNPq and Fapesp, and the Italian Ministero dell'Università e della Ricerca Scientifica e Tecnologica (MURST). R.K.S. acknowledges funding from BASCAL CATA Center for Astrophysics and Associated Technologies PFB-06 and the Ministry for the Economy, Development, and Tourism's Programa Iniciativa Científica Milenio through grant P07-021-F, awarded to The Milky Way Millennium Nucleus.

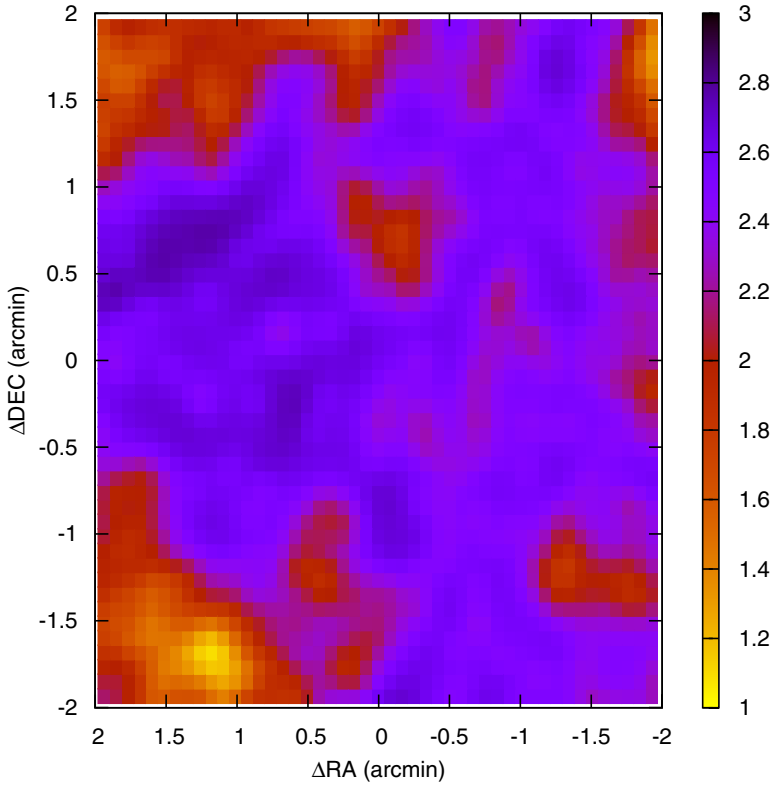

Figure 10. Map showing the distribution of the TNG ($V - I$) mean color in the region of Kronberger 49 (centered at ΔR.A. $= 0, \Delta$decl. $= 0$). North is up and east left.

(A color version of this figure is available in the online journal.)

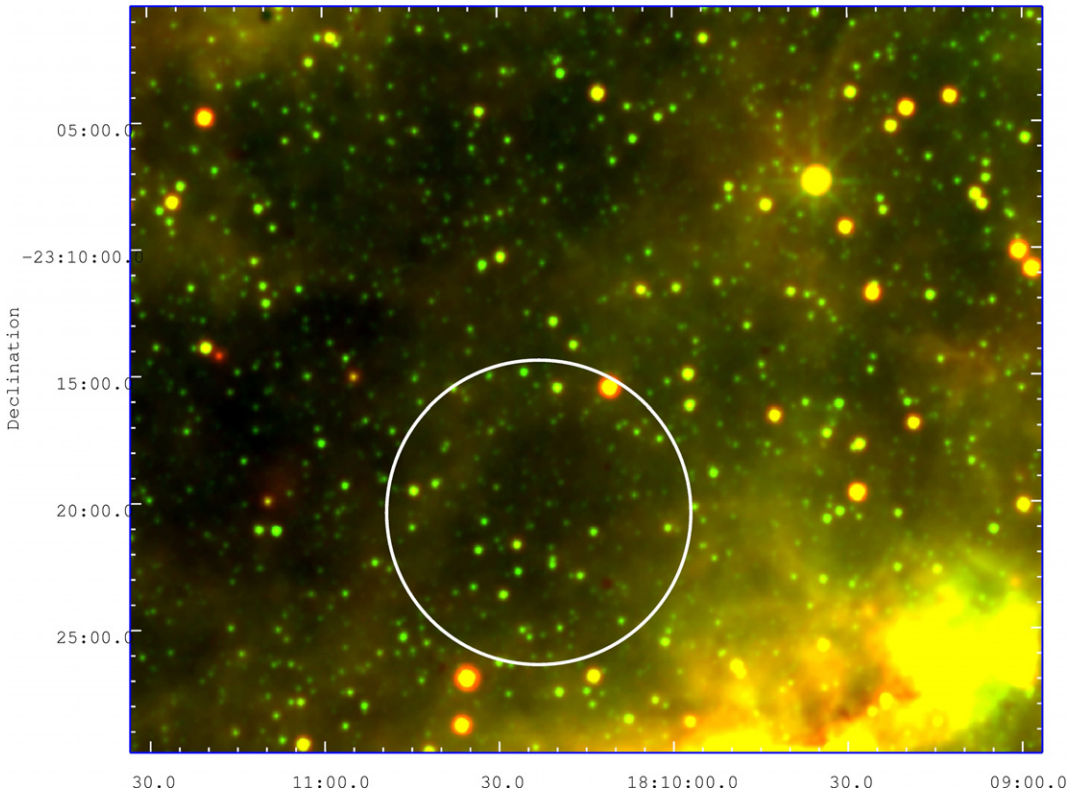

Figure 11. Composite W3 (green) and W4 (red) *WISE* image covering $30' \times 30'$ in the direction of Kronberger 49 (center of the $R = 5'$ circle).
(A color version of this figure is available in the online journal.)

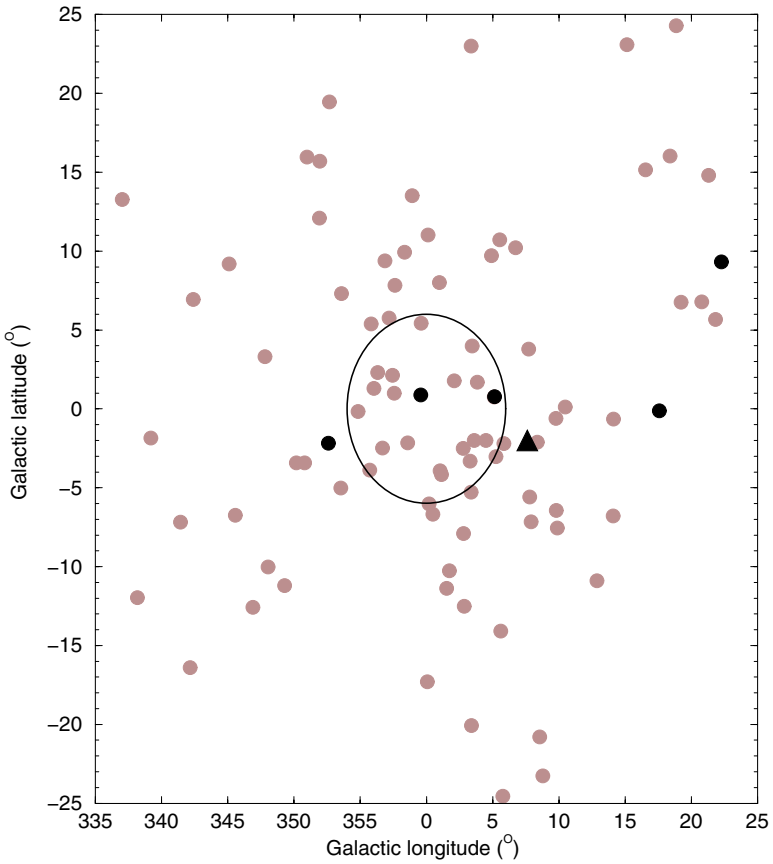

Figure 12. In the case of a globular cluster, Kronberger 49 (filled triangle) is compared to the angular distribution of GCs projected on the central parts of the Galaxy. Those already listed in Harris' catalog are shown as light-shaded symbols, while the recent discoveries/identification are shown with black symbols. The wide circle shows the bulge region studied by Barbuy et al. (1998).

(A color version of this figure is available in the online journal.)

REFERENCES

Andersen, M. I., Freyhammer, L., & Storm, J. 1995, in ESO Conference and Workshop Proceedings, Calibrating and Understanding HST and ESO Instruments Vol. 53, ed. P. Bienvenuti (Garching: ESO), 87

Baade, W., & Gaposchkin, C. H. P. 1963, in Evolution of Stars and Galaxies (Cambridge, MA: Harvard Univ. Press), 277

Barbuy, B., Bica, E., & Ortolani, S. 1998, A&AS, 132, 333

Bonatto, C., & Bica, E. 2007, MNRAS, 377, 1301

Bonatto, C., & Bica, E. 2010, A&A, 516, 81

Bonatto, C., Bica, E., Ortolani, S., & Barbuy, B. 2009, MNRAS, 397, 1032

Dutra, C. M., Santiago, B. X., & Bica, E. L. D. 2002, A&A, 381, 219

Dutra, C. M., Santiago, B. X., Bica, E. L. D., & Barbuy, B. 2003, MNRAS, 338, 253

Fadely, R., Willman, B., Geha, M., et al. 2011, AJ, 142, 88

Gillessen, S., Eisenhauer, F., Fritz, T. K., et al. 2009, ApJ, 707, L114

Gonzalez, O. A., Rejkuba, M., Zoccali, M., et al. 2012, A&A, 543, A13

Harris, W. E. 1996, AJ, 112, 1487 (2010 edition at arXiv:1012.3224)

Inman, R. T., & Carney, B. W. 1987, AJ, 83, 1166

Kronberger, M., Teutsch, P., Alessi, B., et al. 2006, A&A, 447, 921

Landolt, A. U. 1992, AJ, 104, 340

Longmore, A. J., Kurtev, R., Lucas, P. W., et al. 2011, MNRAS, 416, 465

Marigo, P., Girardi, L., Bressan, A., et al. 2008, A&A, 482, 883

Minniti, D., Hempel, M., Toledo, I., et al. 2011, A&A, 527, A81

Minniti, D., Lucas, P. W., Emerson, J. P., et al. 2010, New Astron., 15, 433

Moni, B. C., Mauro, F., Geisler, D., et al. 2011, A&A, 535, A33

Ortolani, S., Barbuy, B., & Bica, E. 1990, A&A, 236, 362

Ortolani, S., Barbuy, B., & Bica, E. 1991, A&A, 249, L31

Ortolani, S., Bica, E., & Barbuy, B. 2006, ApJ, 646, L115

Ortolani, S., Bonatto, C., Bica, E., & Barbuy, B. 2009, AJ, 138, 889

Siegel, M. H., Majewski, S. R., Cudworth, K. M., & Takamiya, M. 2001, AJ, 121, 935

Skrutskie, M., Cutri, R. M., Stiening, R., et al. 2006, AJ, 131, 1163

Stetson, P. B. 1987, PASP, 99, 191

Stetson, P. B. 1994, PASP, 106, 250

Terndrup, D. M. 1988, AJ, 96, 884

The DENIS Consortium 2005, VizieR Online Data Catalog, 2263, 0

Trager, S., King, I. R., & Djorgovski, S. 1995, AJ, 109, 218

Wright., E. L., Eisenhardt, P. R. M., Mainzer, A. K., et al. 2010, AJ, 140, 1868

Zagury, F. 2012, Astron. Nachr., 333, 160